

Study on Photocatalytic Degradation of Rhodamine B by Modified Red Mud Catalyst with Biochar

By Xilin Wang^{1,2}, Dexin Liu^{1,2}

ABSTRACT:

In this work, a red mud(RM)-coffee grounds(CGs) pyrolysis composite material (RC-PC) was prepared and applied to the study of photocatalytic Fenton degradation of organic pollutants. The results of SEM, TEM, and XRD analyses show that during the pyrolysis process, the coffee residue is transformed into biochar with a porous structure, and the hematite in the RM is stepwise reduced to Fe₃O₄ and Fe₀. In the experiment of degrading Rhodamine B (RhB) under simulated visible light conditions, after 30 minutes of reaction, RhB exhibited a degradation efficiency of 94.8% in the light condition, significantly surpassing the 48.8% efficiency observed in the dark Fenton system. Radical quenching experiments and EPR analysis confirmed that hydroxyl radicals (•OH) produced by Fe²⁺-mediated H₂O₂ activation in the photocatalytic Fenton system dominate the degradation of RhB. The results of photogenerated electron-hole quenching experiments indicate that photogenerated holes directly participate in the degradation of RhB by oxidizing OH⁻ ions to generate •OH radicals, and photogenerated electrons participate in the reaction process by promoting the Fe²⁺/Fe³⁺ cycle. Iron leaching from the catalyst induces a homogeneous degradation pathway primarily mediated by Fe²⁺ species during the reaction.

Keywords: red mud; biochar; photo-Fenton

1. Introduction

Water pollution caused by rapid economic growth and large-scale industrialization has become one of the serious threats facing humanity. As a widely used dye, the untreated discharge of RhB can cause severe water pollution. Advanced oxidation processes (AOPs) effectively degrade recalcitrant macromolecular organic pollutants in aquatic systems (Kumari et al., 2023; Guo et al., 2020). Among various advanced oxidation methods, the homogeneous Fenton technology based on Fe²⁺/H₂O₂ degrades organic pollutants by generating •OH (Zhou et al., 2022). Iron sludge production remains a persistent challenge in conventional Fenton processes, significantly impacting their environmental and operational sustainability (Oyekunle et al., 2021). Iron sludge has a high-water content and is difficult to dewater. It adsorbs various pollutants and can easily cause secondary pollution. Traditional landfill disposal offers low resource utilization. Current treatment methods include dewatering and landfilling, stabilization, acid regeneration, and thermal treatment. Resource-oriented approaches, such as producing adsorbents, catalysts, or construction materials, are increasingly emphasized and have become key research focuses. Compared with traditional Fenton oxidation, the synergistic catalytic effect of Fe²⁺ and

¹School of Petroleum Engineering, China University of Petroleum (East China), Qingdao 266580, P. R. China.

²Author 2 Key Laboratory of Unconventional Oil & Gas Development (China University of Petroleum (East China)), Ministry of Education, Qingdao 266580, P. R. China.

light can generate more $\bullet\text{OH}$, enhance the oxidative degradation of organic pollutants, and inhibit the accumulation of iron-containing sludge and reduce the loss of Fe^{2+} (Wang et al. 2022). In recent years, the photocatalytic Fenton reaction based on heterogeneous catalysts has attracted the interest of many researchers (Wu et al. 2023).

Iron oxide stands out among transition metal oxides for photocatalytic applications due to its broad-spectrum visible-light absorption, robust charge-carrier dynamics, and excellent thermodynamic stability. Researchers have demonstrated the efficacy of biomass-derived iron-loaded activated carbon catalysts, with systematic studies optimizing pyrolysis parameters (temperature cycles, residence time) and metal impregnation ratios to enhance redox activity (Zhuang et al., 2017). Babar et al. pyrolyzed almond shell powder at 600 °C for 4 hours, impregnated the biochar with $\text{FeSO}_4 \cdot 7\text{H}_2\text{O}$, and synthesized a Fe/biochar catalyst, which was used to remove methylene blue from aqueous solutions during the catalytic ozonation process. (Babar et al., 2022). As a solid waste with a high iron content, RM can be used as a cheap iron source for the preparation of iron-based Fenton-like catalysts (Feng et al., 2016; Oliveira et al., 2014). Therefore, from the perspectives of environmental protection and energy utilization, the preparation of visible light-responsive catalysts using RM has greater application potential and better environmental benefits.

In this chapter, coffee residue and RM were used as raw materials, and a RM-derived biochar catalyst was prepared by high-temperature pyrolysis in a nitrogen atmosphere. The morphology and structure of the catalyst were characterized by means such as SEM, TEM, and XRD. The effect of this catalyst on activating H_2O_2 to degrade RhB under visible light conditions was studied. Elevated pyrolysis temperatures induced a stepwise reduction of Fe^{3+} species in RM, culminating in the formation of Fe^{2+} and metallic iron (Fe^0) through thermal-driven electron transfer processes. During the carbothermal reduction of Fe_2O_3 , elevated temperatures accelerate the migration and release of lattice oxygen, promoting its stepwise reduction to Fe_3O_4 , FeO , and eventually metallic Fe. At high temperatures, enhanced atomic rearrangement and diffusion facilitate the transformation of Fe_2O_3 into lower-valence iron phases with larger grain sizes and deeper reduction levels, significantly altering its phase composition and microstructure. Through systematic scavenger assays and active species identification, the photocatalytic-Fenton degradation pathways of RhB were elucidated, with hydroxyl radicals ($\bullet\text{OH}$) exhibiting predominant oxidative activity across multiple reaction phases. The roles of photogenerated holes and electrons in the system were verified through experiments. Among them, photogenerated holes accelerated the degradation reaction by oxidizing H_2O to generate $\bullet\text{OH}$, while photogenerated electrons promoted the degradation of RhB in the system by accelerating the $\text{Fe}^{2+}/\text{Fe}^{3+}$ cycle.

2. Material and methods

2.1 Materials

High-purity reagents ($\geq 99.7\%$ certified purity) were utilized across all experimental protocols. RM was sourced from the Jinan Branch of Chalc. The coffee residue was the residue left after brewing common commercial coffee. Rhodamine B (RhB, $\geq 99.0\%$), Hydrogen peroxide (30%), L-histidine (L-His, 99.9%), tert-butanol (TBA, 99.9%), p-benzoquinone (P-BQ, 99.9%), potassium chloride, sodium bicarbonate, and silver nitrate

were purchased from Sinopharm Chemical Reagent Co., Ltd. Hydrochloric acid (37%) was purchased from Yantai Sanhe Chemical Reagent. Anhydrous sodium sulfite was purchased from Tianjin Beilian Fine Chemicals Development Co., Ltd. L-histidine was purchased from Aladdin, and sodium dihydrogen phosphate was purchased from Tianjin Dingshengxin Chemical Co., Ltd.

2.2 Synthesis and characteristics of the catalysts

The RC-PC composite material was synthesized via co-pyrolysis of RM and CGs, leveraging their synergistic interactions during thermal treatment. The RM and coffee residue were dried and then passed through an 80-mesh sieve. A certain proportion of RM and coffee residue was weighed and mixed, and after grinding, it was placed in a tube furnace for high-temperature pyrolysis in a nitrogen atmosphere. The catalysts prepared at pyrolysis temperatures of 750 °C, 800 °C, 850 °C, and 900 °C were denoted as RC-PC750, RC-PC 800, RC-PC 850, and RC-PC 900 respectively. The pyrolysis product of pure coffee residue was prepared and denoted as BC. X-ray diffraction analysis (XRD) was carried out on an X-ray powder diffractometer to determine the crystal structure of the catalyst. The scanning range was from 5° to 85°, with a step size of 0.02°. Material morphology and microstructure were analyzed using SEM (Regulus8100) and TEM (JEM-2100PLUS), while reactive oxygen species (ROS) generation was quantified via EPR spectroscopy (Bruker A200).

2.3 Experimental procedures and analysis

The experiment was conducted in a Pofilei PCX50C multi-channel photocatalytic reaction system. Firstly, 0.003 g of the catalyst was added to a 50 mL solution of RhB with a concentration of 50 mg/L. The concentration of H₂O₂ was 0.1 mmol/L, and the initial pH value of the solution was 3. After the reaction started, the filtrate was filtered out every 5 minutes using a 0.45 μm polytetrafluoroethylene syringe membrane filter, and the absorbance of the solution was measured at a wavelength of 554 nm by an ultraviolet spectrophotometer. TBA, P-BQ, and L-His were used as quenchers for •OH, •O₂⁻, and ¹O₂ respectively, while Na₂SO₃ and AgNO₃ were used as quenchers for photogenerated holes and electrons. Triplicate experiments were conducted, with results expressed as mean values ± standard deviation ranges.

3. Results and discussion

3.1 Catalyst characterizations

Figure 1 presents the X-ray diffraction (XRD) profiles comparing pristine RM with thermally processed catalysts across varying pyrolysis temperatures. The RM has poor crystallinity and complex composition. Among them, the diffraction peaks can be attributed to the characteristic peaks of hematite (Fe₂O₃, PDF#99-0060). When the pyrolysis temperature is 750 °C, the characteristic peaks of hematite in the Fe₃O₄-BC750 catalyst disappear, accompanied by significant changes in the main iron species. At the same time, diffraction peaks of magnetite (Fe₃O₄, PDF#74-0748) appear at 29.7°, 35.0°, 57.0°, and 62.6°, indicating that Fe₂O₃ is reduced to Fe₃O₄ at this temperature. In addition, diffraction peaks of zero-valent iron (Fe⁰, PDF#87-0721) appear at 44.7° and 65.0°, indicating that part of Fe₃O₄ is further reduced to elemental Fe. As the pyrolysis

temperature increases from 750 °C to 800 °C and 900 °C, the intensity of the diffraction peaks of Fe^0 is further enhanced, but there are still diffraction peaks of (Fe_3O_4 , PDF#89-0951) at 29.5° and 34.9°. At 800 °C pyrolysis, a distinct XRD peak emerges at 43.5°, corresponding to the (031) crystallographic plane of Fe_3C (Fe_3C , PDF#71-1174).

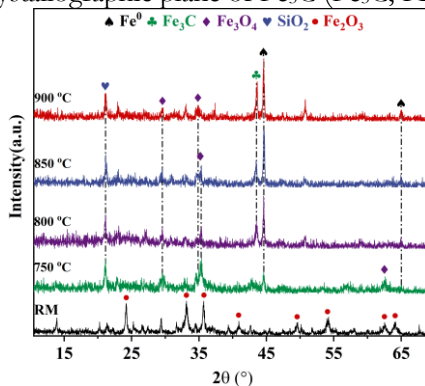


Figure 1: XRD spectra of different RC-PC catalysts.

The surface morphology, elemental composition, and elemental distribution of RC-PC900 were investigated by SEM and EDS. As shown in Figure 2a, the RM-derived catalyst presents irregular particles. Figure 2b shows the elemental composition of the catalyst. Among them, the content of Fe is 12.42 wt%. Figure 2c is the EDS-mapping diagram of the RM-derived catalyst, from which it can be seen that the metallic elements are relatively evenly distributed in the catalyst.

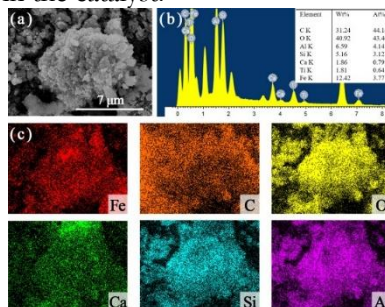


Figure 2: SEM (a), EDS (b), and element mapping (c) of RC-PC900.

The TEM and HRTEM images of RC-PC are shown in Figure 3. It can be seen that the metal particles are uniformly distributed on the surface of the biochar-modified RM catalyst. In Figure 3c, lattice fringes with a spacing of 0.205 nm can be observed, which corresponds to the (110) crystal plane of zero-valent iron, further confirming the formation of elemental iron in the catalyst. In Figure 3d, HRTEM analysis reveals lattice spacings of 0.256 nm and 0.300 nm, matching the d-spacings of magnetite's (311) and (220) planes (Jin et al., 2021; Shahrashoub et al., 2021).

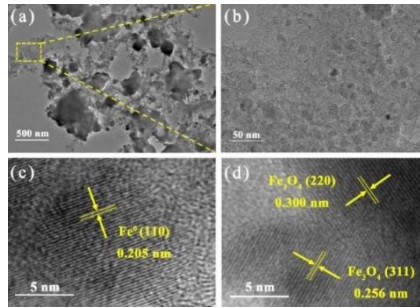


Figure 3: TEM and HRTEM diagrams of RC-PC900.

3.2 Effects of different reaction conditions on degradation

The influence of different concentrations of RhB on the degradation rate is shown in Figure 4a. Elevating the pollutant concentration from 50 to 75 mg/L reduced the degradation efficiency by 35.2% (94.8% to 61.4%) and slowed the reaction kinetics, with the rate constant dropping from 0.081 to 0.034 min⁻¹. This is mainly because the total amount of active species generated in the system is constant, and within the same time period, the degradation efficiency of RhB is inversely proportional to its concentration. As shown in Figure 4b, when the concentration of H₂O₂ increased from 1 mmol/L to 2 mmol/L, the degradation rate of the system increased from 81.7% to 94.8% within 30 minutes. When the concentration of H₂O₂ increased to 4 mmol/L, the increase in the degradation rate was limited, but the initial rate constant increased from 0.081 min⁻¹ to 0.109 min⁻¹, which was quite obvious. In the Fenton system, excessive addition of hydrogen peroxide not only intensifies side reactions between hydroxyl radicals and H₂O₂, reducing oxidation efficiency, but also increases the residual H₂O₂ burden on the ecological environment, posing potential environmental risks and raising treatment costs. Typically, the upper limit for H₂O₂ dosage is twice the COD level of the wastewater.

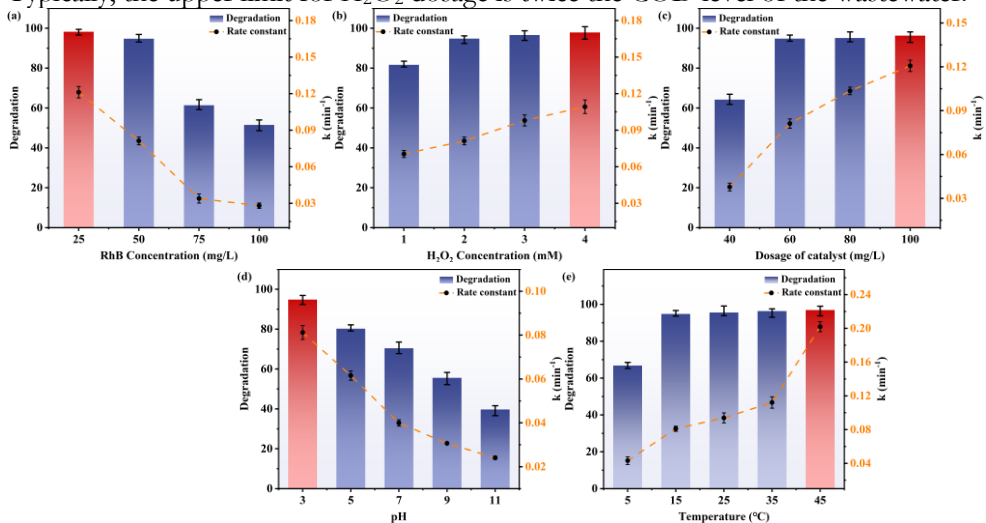


Figure 4: Effect of RhB concentration (a), H₂O₂ concentration (b), catalyst dosage (c), pH value (d), and temperature (e) on degradation of RhB.

The influence of different dosages of the catalyst on the degradation rate is shown in Figure 4c. It can be seen that the degradation rate of RhB increased with the increase in the dosage of the catalyst. Increasing the catalyst dosage from 40 to 60 mg/L enhanced the degradation efficiency by 47.4% (64.3% to 94.8%) and accelerated reaction kinetics, with the rate constant rising from 0.038 to 0.081 min⁻¹. Both increased significantly. This is because the increase in the number of active sites led to an enhancement of the system's ability to activate H₂O₂ to generate active species. Figure 4d shows the influence of different pH values on the degradation rate. The degradation efficiency dropped significantly from 94.8% to 39.7% as pH rose from 3 to 11, demonstrating superior performance in acidic environments for organic pollutant removal. Figure 4e shows the influence of different reaction temperatures on the degradation rate. When the reaction temperature increased from 5 °C to 15 °C, the degradation rate increased from 66.8% to 94.8%. This is mainly because the increase in temperature made it easier for H₂O₂ to be activated to generate active species. Through the linear fitting of the Arrhenius equation, the activation energy of the degradation reaction of RhB was obtained as 22.66 KJ/L.

3.3 Effect of water background on degradation

The background matrix of the water body will also affect the degradation effect of the system on RhB. Cl⁻, HCO₃⁻, and HPO₄²⁻ are common inorganic anions in natural water bodies. In advanced oxidation systems, anions such as Cl⁻, HPO₄²⁻, or HCO₃⁻ can interact with hydroxyl radicals (•OH) at the molecular level through competitive or quenching reactions, forming less reactive radicals such as •Cl⁻ or •CO₃⁻. This interaction weakens the oxidative capacity of ROS toward organic pollutants, significantly affecting the overall degradation efficiency and reaction selectivity of the system.

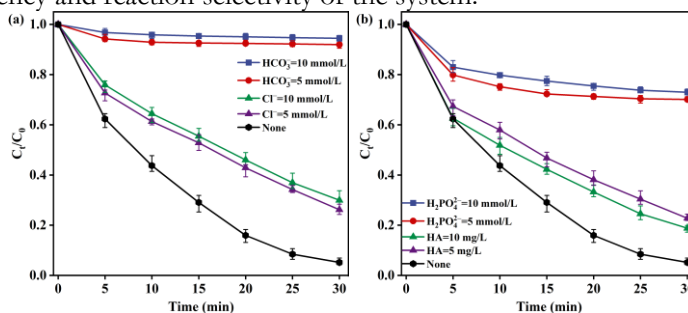


Figure 5: Effect of water background on degradation.

Figures 5a-b show the presence of Cl⁻ significantly inhibits RhB degradation (efficiency drop from 94.8% to 61.4%), confirming •OH as the dominant reactive species in the system. Both HCO₃⁻ and HPO₄²⁻ exhibit a stronger inhibitory effect. The main reason is that the addition of HCO₃⁻ leads to an increase in the pH value of the solution, which in turn affects the degradation efficiency of the system. Moreover, the HPO₄²⁻ present in the system has a better affinity for the coordinatively unsaturated iron species in RC-PC, thus inhibiting the catalyst from activating H₂O₂ to generate ROS, which greatly reduces the degrading efficiency of RhB in the system. Figure 5b demonstrates that natural organic matter (NOM) significantly inhibits RhB degradation, reducing efficiency from 94.8% to 61.4%, likely due to competitive consumption of ROS (•OH/•SO₄⁻) by NOM components. Humic acid (HA) significantly inhibits RhB degradation (efficiency drop

from 94.8% to 61.4%) by competitively scavenging ROS ($\bullet\text{OH}/\bullet\text{SO}_4^-$) and occupying catalytic sites, as confirmed in Fig. 5b. This aligns with studies showing HA's preferential oxidation due to its abundance of phenolic and carboxyl functional groups.

3.4 Research on the mechanism of photo-Fenton reaction

Quenching experiments were conducted on the active species in the light/dark reaction systems using TBA, L-His, and p-BQ, respectively. The quenching results of TBA in the light reaction system are shown in Figure 6a. After introducing TBA with a concentration of 10 mM, the degradation rate of the light reaction system decreased from 94.8% to 21.9%. This quenching results of TBA in the dark reaction system are shown in Figure 6a. TBA also has a significant inhibitory effect on the ability of the dark reaction system to degrade RhB. When the concentration of the introduced TBA is 10 mM, the degradation rate of the dark reaction system decreases to 16.4%. Since the addition of TBA will inhibit the generation of $\bullet\text{OH}$, this result confirms that $\bullet\text{OH}$ makes an important contribution to the degradation of RhB. L-histidine can quench both $\bullet\text{OH}$ and $^1\text{O}_2$ in the system at the same time. By comparing the results of its quenching experiment with that of TBA, the contribution of $^1\text{O}_2$ to the degradation of RhB by the system can be verified. The quenching experiment results of L-histidine are shown in Figure 6b. Under the light reaction conditions, after adding L-histidine, the degradation rate of the system decreased from 94.8% to 7.6%. After adding L-histidine under the dark reaction conditions, the degradation rate of the system decreased from 48.4% to 4.3%. This result proves that $^1\text{O}_2$ is also involved in the degradation of RhB. p-Benzoquinone was introduced to quench $\bullet\text{O}_2^-$ to verify the contribution of $\bullet\text{O}_2^-$ to the degradation of RhB. The quenching experiment results are shown in Figure 6c. After adding 1 mM of p-benzoquinone, the degradation rate of the photo-Fenton system decreased from 94.8% to 86.9%. When the concentration of p-benzoquinone was further increased to 10 mM, the degradation rate of the system at 15 minutes instead increased from 70.9% to 89.4%. To accurately verify the contribution of $\bullet\text{O}_2^-$ to the degradation of RhB, both L-histidine and p-benzoquinone were added to the system simultaneously. Among them, L-histidine has a strong quenching effect on $\bullet\text{OH}$ and can eliminate the effect of the increase in $\bullet\text{OH}$ in the system caused by the addition of p-benzoquinone. The quenching results are shown in Figure 6d. When L-histidine and p-benzoquinone were added simultaneously, the degradation rate of the light reaction system decreased from 94.8% to 5.9%, and the degradation rate of the dark reaction system decreased from 48.4% to 2.4%. By comparing with the results of the L-histidine quenching experiment, it can be seen that $\bullet\text{O}_2^-$ makes little contribution to the degradation of RhB in the system. To further quantitatively determine the contributions of various ROS, the apparent rate constants of the reaction when TBA, L-histidine, and L-histidine + p-benzoquinone were added were calculated as k_1 , k_2 , and k_3 respectively, and the reaction rate constant without adding a quencher was k_0 . The relative contributions of $\bullet\text{OH}$, $^1\text{O}_2$, and $\bullet\text{O}_2^-$ were calculated according to Eq 1-3.

$$\lambda(\bullet\text{OH}) = (k_0 - k_1)/k_0 \quad \text{Eq 1}$$

$$\lambda(^1\text{O}_2) = (k_1 - k_2)/k_0 \quad \text{Eq 2}$$

$$\lambda(\bullet\text{O}_2^-) = (k_3 - k_2)/k_0 \quad \text{Eq 3}$$

Among them, $\lambda(\bullet\text{OH})$, $\lambda(^1\text{O}_2)$, and $\lambda(\bullet\text{O}_2^-)$ are the contributions of $\bullet\text{OH}$, $^1\text{O}_2$, and $\bullet\text{O}_2^-$ in the system to the degradation of RhB. As shown in Figure 6e, in the light reaction

system, k_0 , k_1 , k_2 , and k_3 are 0.0887, 0.0085, 0.0036, and 0.0028 min^{-1} respectively. Through the formula, it can be calculated that the contribution rates of $\bullet\text{OH}$, $^1\text{O}_2$, and $\bullet\text{O}_2^-$ in the RC-PC photo-Fenton system are 90.4%, 5.5%, and 0.9% respectively. As shown in Figure 6f, in the dark reaction system, k_0 , k_1 , k_2 , and k_3 are 0.0294, 0.0076, 0.0021, and 0.0011 min^{-1} respectively. It can be calculated that the contribution rates of $\bullet\text{OH}$, $^1\text{O}_2$, and $\bullet\text{O}_2^-$ in the RC-PC dark Fenton system are 74.1%, 18.7%, and 3.4% respectively.

Both photo-Fenton and dark Fenton systems rely primarily on $\bullet\text{OH}$ for degradation, with $^1\text{O}_2$ serving as a secondary reactive species. The role of $\bullet\text{O}_2^-$ is minimal, particularly negligible in photo-Fenton systems. Comparative studies reveal that $\bullet\text{OH}$ generation is significantly enhanced under photo-Fenton conditions versus dark Fenton, attributed to accelerated $\text{Fe}^{2+}/\text{Fe}^{3+}$ cycling via photogenerated electrons. The main reason is that in the photo-Fenton system, the photogenerated electrons and holes promote the $\text{Fe}^{2+}/\text{Fe}^{3+}$ cycle respectively and directly oxidize H_2O to generate $\bullet\text{OH}$, which increases the amount of $\bullet\text{OH}$ in the system. However, the generation of $^1\text{O}_2$ is mainly related to O_2 , and the photogenerated electrons and holes have no effect on the generation of $^1\text{O}_2$. The photo-Fenton system exhibits higher $\bullet\text{OH}$ yield than dark Fenton due to accelerated $\text{Fe}^{2+}/\text{Fe}^{3+}$ cycling via photogenerated electrons (Sun et al., 2021; Li et al., 2019).

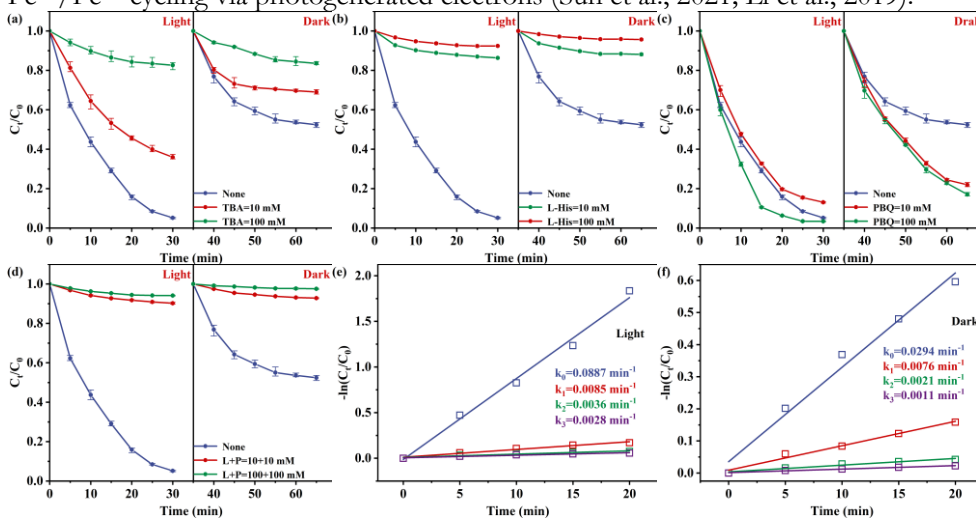


Figure 6: Effect of TBA (a), L-His (b), PBQ (c), and L-His+PBQ (d) on degradation, reaction kinetics curves (e-f).

The results of the photogenerated electron-hole quenching experiment are shown in Figure 7. It can be seen that the addition of Na_2SO_3 has a significant inhibitory effect on the degradation of RhB in the photo-Fenton system, and the degradation rate decreases from 94.8% to 71.7%. Since the results of the L-histidine quenching experiment have confirmed that $\bullet\text{OH}$ plays an important role in the degradation of RhB, the photogenerated holes generated in the system do not directly react with RhB for oxidation, but AgNO_3 addition reduced RhB degradation efficiency from 94.8% to 63.8% in the photo-Fenton system, demonstrating photogenerated electrons' critical role in $\bullet\text{OH}$ generation via OH^- activation (Xing et al., 2020). This aligns with studies showing electron-trapping effect of Ag^+ that disrupts $\text{Fe}^{2+}/\text{Fe}^{3+}$ redox cycling. The p-benzoquinone quenching experiment has confirmed that $\bullet\text{O}_2^-$ has only a weak effect on

the degradation of RhB. Therefore, the photogenerated electrons in the system participate in the degradation of RhB by accelerating the $\text{Fe}^{2+}/\text{Fe}^{3+}$ cycle.

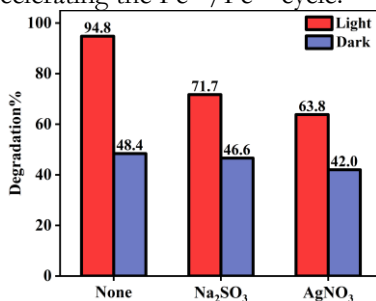


Figure 7: Effect of photogenic produces electron-holes on degradation.

To explore the contribution of ROS in the system, this work used EPR testing to study the ROS generated during the degradation process. As shown in Figure 8a, no signal was detected in the $\text{RM} + \text{H}_2\text{O}_2$ system. This result indicates that RM cannot activate H_2O_2 alone to generate ROS, and it only has catalytic activity after carbothermal reduction. In addition, an obvious $\bullet\text{OH}$ signal can be detected in the $\text{RC-PC} + \text{H}_2\text{O}_2$ system, but the intensity is much lower than the $\bullet\text{OH}$ signal detected in the $\text{RM} + \text{H}_2\text{O}_2 + \text{Light}$ system, indicating that the photo-Fenton system can generate more $\bullet\text{OH}$ for the degradation of RhB. Using TEMP as the trapping agent, the $^1\text{O}_2$ signal in the system was detected. The results are shown in Figure 8b. No signal was detected in the $\text{RM} + \text{H}_2\text{O}_2$ system, while $^1\text{O}_2$ signals with comparable intensities were detected in both the $\text{RC-PC} + \text{H}_2\text{O}_2$ and $\text{RM} + \text{H}_2\text{O}_2 + \text{Light}$ systems, which indicates that the photo-Fenton system does not promote the generation of $^1\text{O}_2$. This phenomenon is comply with the photogenerated electron-hole quenching experiment result, proving that the photogenerated carriers promote the degradation reaction of RhB by accelerating the generation of $\bullet\text{OH}$ rather than other ROS.

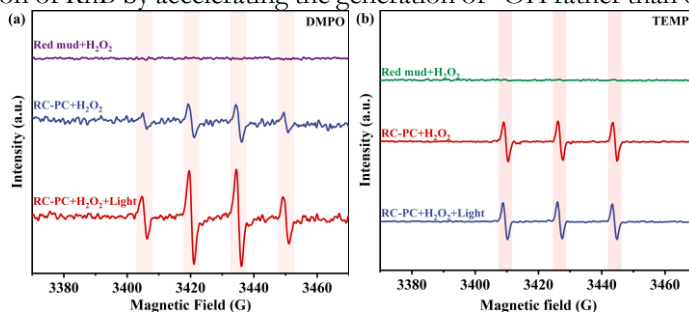


Figure 8: EPR spectra in activation of H_2O_2 with RM, RC-PC, RC-PC+Light using DMPO (a) and TEMP (b) as the trapping agents.

3.5 Stability experiment of RC-PC

A reusability test was conducted on the catalyst to measure the RC-PC's stability in the light condition, and the reaction conditions were the same as those described previously. Post-reaction, the RC-PC composite underwent sequential washing with deionized water and ethanol (3 times), followed by oven-drying at 60°C for repeatability testing. The experimental results are shown in Figures 9 a-b. After five consecutive reactions, the degradation rate of RhB in the photo-Fenton system at 30 minutes decreased

from 94.7% to 72.4%, and the degradation rate in the Fenton system decreased from 48.4% to 17.6%. Under acidic conditions, part of the Fe^{2+} in RC-PC leached into the system and participated in the degradation process of RhB through homogeneous catalysis by Fe^{2+} . This part of Fe^{2+} was converted into Fe^{3+} after activating H_2O_2 and dispersed in the solution, and could not be reduced by the subsequently generated photogenerated electrons, which reduced the cycle efficiency of $\text{Fe}^{2+}/\text{Fe}^{3+}$. This is the main reason for the decrease in the catalytic performance of RC-PC after multiple repetitions. To verify the leaching effect of Fe^{2+} , a control group, and a leaching group were set up. 0.06 g/L of RC-PC was placed in a RhB solution with a pH of 3 and a concentration of 50 mg/L and left standing for 30 minutes. After Fe^{2+} was fully leached, RC-PC was recovered to obtain the leaching system. Then, 1 mM of H_2O_2 was added to the leaching system to initiate the degradation reaction. The experimental results are shown in Figure 9c. The degradation rate of RhB in the RC-PC leaching system was 42.2%, which proves that Fe^{2+} in RC-PC was successfully leached under acidic conditions. The leaching system is a homogeneous catalytic system dominated by Fe^{2+} . This system reacts rapidly, but its subsequent degradation ability is weak due to the lack of the $\text{Fe}^{2+}/\text{Fe}^{3+}$ cycle. The leaching experiment shows that homogeneous and heterogeneous reactions coexist in the RC-PC photo-Fenton system. The leached Fe^{2+} activates H_2O_2 to generate $\bullet\text{OH}$, which participates in the degradation of RhB, and this process is a homogeneous reaction. At the same time, the non-leached Fe^{2+} activates H_2O_2 to generate various free radicals, the photogenerated electrons promote the $\text{Fe}^{2+}/\text{Fe}^{3+}$ cycle, and the photogenerated holes activate H_2O to generate $\bullet\text{OH}$. The combined action of homogeneous and heterogeneous reactions endows the RC-PC photo-Fenton system with a strong degradation ability for organic pollutants.

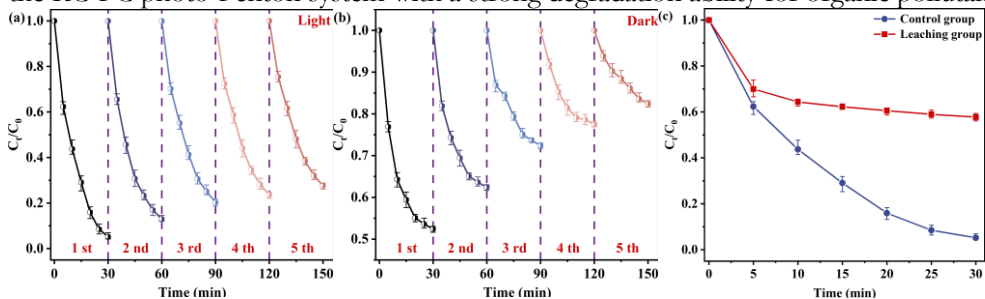


Figure 9: Cyclic experiments of light Fenton system (a) and Fenton system (b); Fe^{2+} leaching experiment (c).

4. Conclusion

Pyrolyzing RM after mixing it with CGs is conducive to the transformation of hematite into magnetite and the formation of biochar with a porous structure, thus preparing an RC-PC catalyst with a highly efficient photocatalytic capability. The research results of XRD, SEM, and TEM show that the pyrolysis temperature determines the final conversion product of hematite and the surface pore distribution of the biochar. In the RhB degradation experiment, simulating visible light conditions can improve RC-PC's performance. The results of free radical and photogenerated electron-hole quenching experiments, as well as EPR results, confirms $\bullet\text{OH}$ as the dominant reactive species

responsible for RhB degradation. Photogenerated holes directly participate in the degradation of RhB by oxidizing H₂O to generate •OH and photogenerated electrons participate in the reaction process by promoting the Fe²⁺/Fe³⁺ cycle.

References

- Babar, M., Munir, H. M. S., Nawaz, A., Ramzan, N., Azhar, U., Sagir, M., & Chew, K. W. (2022): Comparative study of ozonation and ozonation catalyzed by Fe-loaded biochar as catalyst to remove methylene blue from aqueous solution. *Chemosphere*, 307, 135738.
- Feng, Y., Wu, D., Liao, C., Deng, Y., Zhang, T., & Shih, K. (2016): RM powders as low-cost and efficient catalysts for persulfate activation: pathways and reusability of mineralizing sulfadiazine. *Separation and Purification Technology*, 167, 136-145.
- Guo, K., Zheng, S., Zhang, X., Zhao, L., Ji, S., Chen, C., & Fang, J. (2020): Roles of bromine radicals and hydroxyl radicals in the degradation of micropollutants by the UV/bromine process. *Environmental Science & Technology*, 54(10), 6415-6426.
- Jin, J., Liu, X., Yuan, S., Gao, P., Li, Y., Zhang, H., & Meng, X. (2021): Innovative utilization of red mud through co-roasting with coal gangue for separation of iron and aluminum minerals. *Journal of Industrial and Engineering Chemistry*, 98, 298-307.
- Li, Y., Wei, G., Shao, L., Li, Z., Yu, F., Liu, J., & Zhang, L. (2019): Green synthesis of red mud-based ZnO single Fe₂O₃ composite used for photo-Fenton reaction under visible light. *Journal of Cleaner Production*, 207, 717-727.
- Kumari, H., Sonia, Suman, Ranga, R., Chahal, S., Devi, S., & Parmar, R. (2023): A review on photocatalysis used for wastewater treatment: dye degradation. *Water, Air, & Soil Pollution*, 234(6), 349.
- Oliveira, A. A. S., Teixeira, I. F., Christofani, Tais, Tristão, J. C., Guimarães, I. R., & Moura, F. C. C. (2014): Biphasic oxidation reactions promoted by amphiphilic catalysts based on red mud residue. *Applied Catalysis B Environmental*, 144, 144-151.
- Oyekunle, D. T., Zhou, X., Shahzad, A., & Chen, Z. (2021): Review on carbonaceous materials as persulfate activators: structure-performance relationship, mechanism and future perspectives on water treatment. *Journal of Materials Chemistry A*, 9(13), 8012-8050.
- Shahrashoub, M., Bakhtiari, S., Afroosheh, F., & Googheri, M. S. (2021): Recovery of iron from direct reduction iron sludge and biosynthesis of magnetite nanoparticles using green tea extract. *Colloids and Surfaces A: Physicochemical and Engineering Aspects*, 622(3), 126675.
- Sun, R., Zhang, X., Wang, C., & Cao, Y. (2021): Co-carbonization of red mud and waste sawdust for functional application as Fenton catalyst: evaluation of catalytic activity and mechanism. *Journal of Environmental Chemical Engineering*, 9(4), 105368.
- Xing, W., Zhou, L., Chen, B., Lei, J., Wang, L., & Zhang, J. (2020): α - FeOOH-MoO₃ nanorod for effective photo - Fenton degradation of dyes and antibiotics at a wide range of pH. *Chemistry-An Asian Journal*, 15(17), 2749-2753.
- Wang, S., An, W., Lu, J., Liu, L., Hu, J., Liang, Y., & Cui, W. (2022): A Cu/CuFe₂O₄-OVs two-electron center-based synergistic photocatalysis-Fenton system for efficient degradation of organic pollutants. *Chemical Engineering Journal*, 441, 135944.
- Wu, Q., Siddique, M. S., Wang, H., Cui, L., Wang, H., Pan, M., & Yan, J. (2023): Visible-light-driven iron-based heterogeneous photo-Fenton catalysts for wastewater decontamination: a review of recent advances. *Chemosphere*, 313, 13750.
- Zhou, Y., He, J., Li, X., Lu, J., & Zhou, Y. (2022): Efficient removal of roxarsone and emerging organic contaminants by a solar light-driven in-situ Fenton system. *Chemical Engineering Journal*, 435, 132434.
- Zhuang, H., Huang, H., Xu, K., Zhang, Y., Yuan, X., & Han, H. (2017): Advanced treatment of paper-making wastewater by heterogeneous catalytic ozonation. *Industrial Water Treatment*, 37(6), 30.